Chapter 15
Shaker Capability Estimation Through Experimental Dynamic Substructuring

Peter Fickenwirth, John Schultze, Dustin Harvey, and Michael Todd

Abstract Electrodynamic shaker systems are a staple in shock and vibration environments testing, yet the specific performance limits of these systems are not well characterized. Manufacturer ratings give a general idea of a system's capability, but the details of their performance remain uncharacterized, often leaving test engineers using their best judgment to determine if a test is feasible. This work applies dynamic substructuring to better predict shaker capability throughout the system's full range. By modeling a shaker system, insight is gained into the potential performance, but the difficulty remains that the dynamics of the system will change depending on how the test configuration is defined. If no analytical model of the article exists, it is challenging to make evaluations of the new coupled system's behavior. An experimental model of the test article is developed through modal impact testing, without the need of a shaker. This experimental model is then coupled to a 4-DOF lumped-parameter electromechanical shaker model through dynamic substructuring. The coupled system can then be used for shaker capability estimation for a specific test configuration. By utilizing a modal test and substructuring to estimate performance, no time is lost with the article on the shaker determining if a test specification is achievable. Beyond time savings, the modal model could be coupled to multiple shaker models to determine the best machine for a given test.

Keywords Dynamic substructuring · Environments testing · Modal testing

15.1 Introduction

Historically, equipment for vibration testing of assemblies has been selected based on past tests, engineering judgment, and simple calculations using Newton's second law of physics. However, the electrodynamic shaker systems used to perform these tests have complicated dynamics, and there are many variables to consider when predicting a system's capability. The device under test (DUT) and its various orientations being tested, the fixturing required for testing, the shaker and amplifier used, and even the software used to control the system all influence the dynamics of the shaker. These dynamics in turn affect its capability to achieve the specified mechanical outputs. A more detailed understanding of these systems can be achieved through modeling of the shaker itself. Updating the model with experimentally collected data further ensures an accurate characterization of its performance. However, more information is needed still, as the setup of the test on the shaker may strongly influence the dynamics of the now coupled system. Modal testing can relatively quickly characterize the dynamics of a device under test, which can then be coupled to the shaker model through dynamic substructuring to achieve a full understanding of the coupled system.

P. Fickenwirth (✉) · J. Schultze · D. Harvey
Los Alamos National Laboratory, Test Engineering Group, Los Alamos, NM, USA
e-mail: pfickenwirth@lanl.gov

M. Todd
University of California, San Diego, Department of Structural Engineering, Los Alamos National Laboratory, Los Alamos, NM, USA

J. Harvie (ed.), *Dynamic Environments Testing, Volume 7*, Conference Proceedings of the Society for Experimental Mechanics Series, https://doi.org/10.1007/978-3-031-34930-0_15

15.2 Background

15.2.1 Shaker Modeling

Many modeling approaches have been taken to capture the dynamics of electrodynamic shaker systems. All of these models seek to characterize the fundamental modes of a shaker system. These are the isolation mode, where the shaker entirely moves together on its isolation mounts, the suspension mode, where the armature moves in opposition to the body, and the coil mode, where the armature table and coil move in opposition to one another [1]. Figure 15.1 shows a diagram of a typical electrodynamic shaker.

Most modeling approaches use a lumped parameter model with anywhere from 2 mechanical degrees of freedom (DoFs) up to 6, all with one additional electrical degree of freedom. Both Schultz [2] and Mayes et al. [3] used 4-DOFs, modeling the shaker body, armature, and a mass on the end of a stinger. Many others modeled the voice coil of the shaker and armature table as two separate degrees of freedom, such as Ricci and Peeters [4], as well as Manzato et al. [5], in their work on virtual shaker testing. Other approaches sought to make an impedance model, with Smallwood using a two-port network model to represent the shaker as an impedance matrix [6], and Tiwari et al. utilizing a 4-DOF lumped parameter model but using the impedance analogy to develop an equivalent electrical model [7]. Some models ignore the motion of the body and, therefore, the isolation mode, as some shakers are rigidly attached to the ground, or to a mass so large that the natural frequency of the isolation mode is too low to practically characterize [8, 9]. Models that utilized more degrees of freedom attempted to characterize some of the out-of-axis motion of the shaker table, with Hoffait et al. modeling the table with rotational degrees of freedom [10].

15.2.2 Experimental Dynamic Substructuring

Dynamic substructuring is the set of techniques used to break down a large, complex dynamic system into substructures for higher fidelity modeling and analysis, while still preserving the overall dynamics of the system. These techniques are commonly applied to finite element analysis models to save time by modeling substructures separately and reassembling the results later. In experimental analysis, substructuring is used to test substructures separately, characterize local dynamics, and then assess their contributions to system-level dynamics. One of the most powerful applications of dynamic substructuring is the ability to combine analytical and experimental analyses of substructures into a full model together [11].

Dynamic substructuring can be represented and applied in many domains, but for this work, the focus is on the frequency domain. Specifically, the Lagrange-multiplier frequency-based-substructuring method (LM-FBS) is used, as described by de

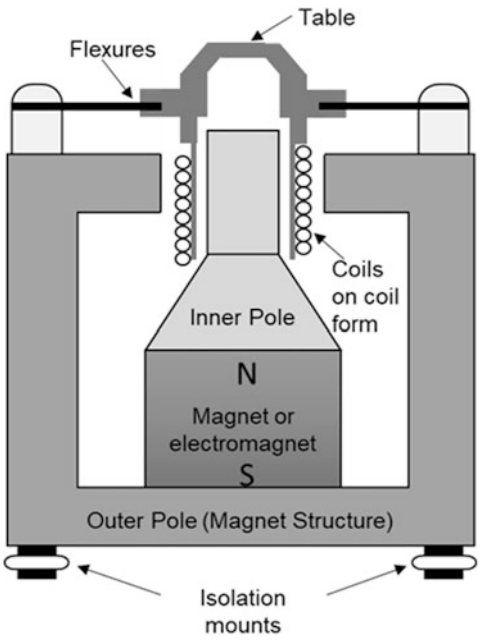

Fig. 15.1 Diagram of an electrodynamic shaker

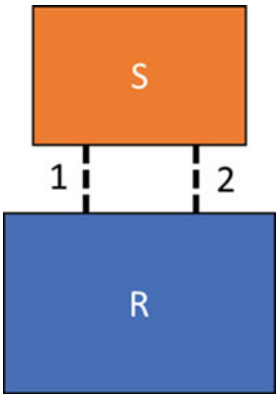

Fig. 15.2 Example of two substructures, *S* and *R*, coupled together at two locations, 1 and 2

Klerk et al. [12], who showed that this method of frequency-based substructuring is equivalent to the classical FBS developed by Jetmundsen [13], but in a simpler form. Consider two substructures, S and R, to be coupled together at two locations, 1 and 2, as shown in Fig. 15.2.

Two interface conditions must be satisfied to assemble the substructures together and understand their coupled dynamics: compatibility and equilibrium. The compatibility condition requires that the responses at the degrees of freedom on either side of the interface between the two substructures must be equal. The equilibrium condition requires that the sum of the internal forces, the forces imparted by the substructures on one another at the interface, must be zero when assembled. A signed Boolean mapping matrix, **B**, is defined by how the substructures are coupled. The matrix can be defined as two submatrices, one for each substructure, that is then concatenated.

$$\mathbf{B}^{\mathrm{S}} = \begin{matrix} \\ 1 \\ 2 \end{matrix} \overset{\begin{matrix} \mathrm{S}_i & \mathrm{S}_{b1} & \mathrm{S}_{b2} \end{matrix}}{\begin{bmatrix} 0 & \mathrm{I} & 0 \\ 0 & 0 & \mathrm{I} \end{bmatrix}}, \mathbf{B}^{\mathrm{R}} = \overset{\begin{matrix} \mathrm{R}_i & \mathrm{R}_{b1} & \mathrm{R}_{b2} \end{matrix}}{\begin{bmatrix} 0 & -\mathrm{I} & 0 \\ 0 & 0 & -\mathrm{I} \end{bmatrix}} \tag{15.1}$$

$$\mathbf{B} = \left[\mathbf{B}^{\mathrm{S}}, \mathbf{B}^{\mathrm{R}}\right] \tag{15.2}$$

The columns of **B** are the degrees of freedom of the substructures with S_{i} and R_i being the internal degrees of freedom of each substructure, S_{b1} and R_{b1} the degrees of freedom on interface 1, and S_{b2} and R_{b2} the degrees of freedom on interface 2. The non-zero elements indicate which DOFs are at connections. The rows are the interfaces where those DOFs are connected. The compatibility condition can then be written using this matrix as

$$\mathbf{Bu} = \mathbf{0} \tag{15.3}$$

Where **u** is the vector of all responses at the interfaces. The LM-FBS method utilizes a dual assembly approach, which introduces interface forces **g**, that automatically satisfy the equilibrium condition.

$$\mathbf{g} = -\mathbf{B}^{\mathrm{T}}\boldsymbol{\lambda} \tag{15.4}$$

This definition for the interface forces can then be substituted into the dynamic equilibrium equation.

$$\mathbf{u} = \mathbf{Y}\left(\mathbf{f} - \mathbf{B}^{\mathrm{T}}\boldsymbol{\lambda}\right) \tag{15.5}$$

Where **Y** is the frequency response matrices of the two substructures assembled blockwise diagonally. Substituting this definition of **u** into the compatibility condition in Eq. 15.3 and then simplifying, $\boldsymbol{\lambda}$ can be determined.

$$\boldsymbol{\lambda} = \left(\mathbf{BYB}^{\mathrm{T}}\right)^{-1}\mathbf{BYf} \tag{15.6}$$

This definition of $\boldsymbol{\lambda}$ can be substituted into the dynamic equilibrium Eq. 15.5 and simplified again.

$$\mathbf{u} = \left(\mathbf{Y} - \mathbf{YB}^{\mathbf{T}}\left(\mathbf{BYB}^{\mathbf{T}}\right)^{-1}\mathbf{BY}\right)\mathbf{f} \tag{15.7}$$

Equation 15.5 defines the dynamic equilibrium of the fully coupled system. The new coupled FRF matrix $\mathbf{Y}_{\text{dual}}$ can then be defined.

$$\mathbf{Y}_{\mathbf{coupled,dual}} = \mathbf{Y} - \mathbf{YB}^{\mathbf{T}}\left(\mathbf{BYB}^{\mathbf{T}}\right)^{-1}\mathbf{BY} \tag{15.8}$$

Equation 15.6 is the formula for LM-FBS and defines the FRF matrix of the fully coupled system. $\mathbf{Y}_{\text{dual}}$ is defined for all the local DOFs on all the substructures and, therefore, contains redundant information at the DOFs that have been coupled. To utilize the LM-FBS formula, driving point FRFs are required for every DOF coupled together, as well as at any other DOFs of interest.

15.3 Shaker Model Development

A 4-DOF lumped parameter electromechanical model for the shakers was chosen. This model was chosen because it captures the dynamics of the three main modes of a shaker system but is simple enough to develop by hand and computationally easy to implement. This 4-DOF model appeared multiple times in the literature and proved to capture the dominant dynamics of most shaker systems. The model consists of three mechanical DOFs, the body of the shaker, the armature table, and the armature coil. These are elastically connected to one another with springs and dampers. The fourth DOF is the charge in the electrical component of the system. The circuit consists of a source EMF, an inductor, and a resistor. The two models are connected by the force imparted on the mechanical system, which is proportional to the current, and the corresponding back EMF on the electrical system, which is proportional to the relative velocity of the body and coil. A diagram of the model is shown in Fig. 15.3.

The model consists of 12 parameters. The mechanical side contains three masses, M_b, M_t, and M_c, three stiffnesses, k_b, k_t, and k_c, and three dampings, c_b, c_t, and c_c. The electrical model contains the resistance of the coil, R, and the inductance, I. Lastly, the two systems are coupled together by the coupling factors, which are replaced with a single constant K. These

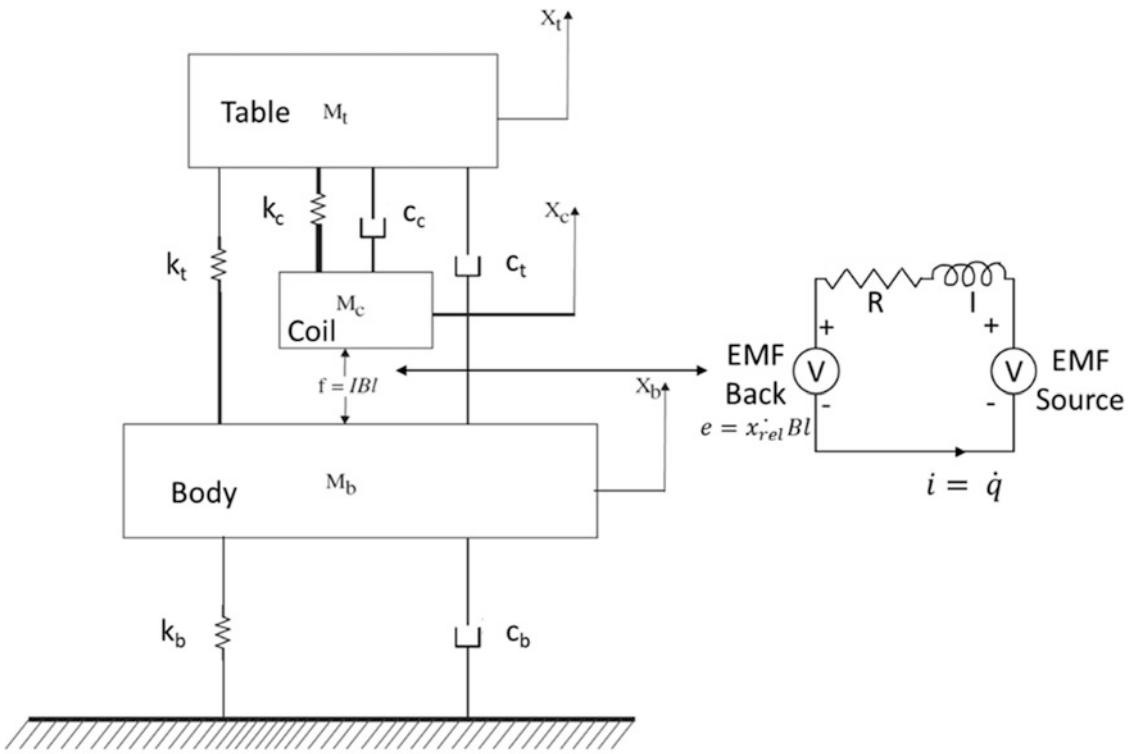

Fig. 15.3 Shaker electromechanical model diagram

factors are only equal if SI units are used. Of these 12 parameters, 5 were determined from the specification sheet provided by the shaker manufacturer and measurements made on the system. The shaker's body mass and armature mass, the sum of both the table and coil, and the flexure stiffness, *kt*, were available. The resistance of the coil was measurable directly on the shaker input terminal. The remaining parameters must be estimated through measurements on the system itself.

The end-use of this model is ultimately FBS, which couples together the frequency response functions (FRFs) of two different substructures to determine their coupled dynamics. Therefore, the FRFs of interest for this model must be calculated from it. First the equations of motion of the system were assembled based on the model. The displacements of the body, table, and coil are the mechanical DOFs and charge is chosen as the electrical DOF, so that the time-derivatives of the DOFs remain consistent.

$$\begin{bmatrix} M_b & 0 & 0 & 0 \\ 0 & M_t & 0 & 0 \\ 0 & 0 & M_c & 0 \\ 0 & 0 & 0 & L \end{bmatrix} \begin{Bmatrix} \ddot{x}_b \\ \ddot{x}_t \\ \ddot{x}_c \\ \ddot{q} \end{Bmatrix} + \begin{bmatrix} c_b + c_t & -c_t & 0 & K \\ -c_t & c_t + c_c & -c_c & 0 \\ 0 & -c_c & c_c & -K \\ -K & 0 & K & R \end{bmatrix} \begin{Bmatrix} \dot{x}_b \\ \dot{x}_t \\ \dot{x}_c \\ \dot{q} \end{Bmatrix} + \begin{bmatrix} k_b + k_t & -k_t & 0 & 0 \\ -k_t & k_t + k_c & -k_c & 0 \\ 0 & -k_c & k_c & 0 \\ 0 & 0 & 0 & 0 \end{bmatrix} \begin{Bmatrix} x_b \\ x_t \\ x_c \\ q \end{Bmatrix} = \begin{Bmatrix} f_b \\ f_t \\ f_c \\ E \end{Bmatrix} \tag{15.9}$$

If the matrices are then denoted **M**, **C**, and **K** respectively, the vector of response DOFs is denoted **x**, and the vector of input forces **f**, the system can efficiently be written in a familiar form.

$$\boldsymbol{M}\ddot{\boldsymbol{x}} + \boldsymbol{C}\dot{\boldsymbol{x}} + \boldsymbol{K}\boldsymbol{x} = \boldsymbol{f} \tag{15.10}$$

From Eq. 15.9 and its restatement as Eq. 15.10, the FRFs of the system can be easily calculated using the direct frequency response method.

$$\boldsymbol{H} = \left(-\omega^2 \boldsymbol{M} + j\omega \boldsymbol{C} + \boldsymbol{K}\right)^{-1} \tag{15.11}$$

Where *H* is the frequency response function matrix of the full system. H is calculated on a frequency line basis, with ω being the frequency, in radians, at that line. The result is 4×4×n matrix, where n is the number of frequency lines calculated. There are no input forces on the mechanical degrees of freedom, so only the fourth column of FRFs is needed, which are the responses to an electrical input, *E*. The impedance of the shaker is calculated from the electrical DOF, while the acceleration-voltage FRF is derived from the table DOF. The acceleration-current FRF is the product of the acceleration-voltage FRF and the impedance.

The three FRFs of interest are affected by each of the parameters in the model. A parameter sensitivity study was performed to understand how changes in these parameters manifest in the FRFs. A baseline value was chosen for each of the parameters and held constant throughout. Then, one parameter at a time was subjected to an upward and downward perturbation. After completing the perturbations for each of the parameters, the effects on the FRFs were assembled into Table 15.1, as well as the expected source for that parameter value. While the effects on all three FRFs were viewed, the effects in Table 15.1 focus on the shaker's impedance.

Table 15.1 Model parameter sensitivities

Parameter	Source	Effect on impedance
M_b – Shaker body mass	Spec sheet	Shifts frequency of isolation mode
M_t – Table mass	Spec sheet, estimate$M_t + M_c = M_{\text{armature}}$	Shifts frequency of isolation mode and suspension mode
M_c – Coil mass	Spec sheet, estimate$M_t + M_c = M_{\text{armature}}$	Shifts frequency of isolation mode and coil mode
C_b – Isolation mount damping	Estimate	Shifts amplitude of isolation mode
C_t – Flexure damping	Estimate	Shifts amplitude of suspension mode
C_c – Coil damping	Estimate	Shifts amplitude of suspension mode and coil mode
K_b – Isolation mount stiffness	Estimate	Shifts frequency of isolation mode
K_t – Flexure stiffness	Spec sheet	Shifts frequency of suspension mode
K_c – Coil stiffness	Estimate	Shifts frequency of suspension mode, slightly coil mode
R – Coil resistance	Measure	Shifts overall amplitude slightly, significantly shifts coil mode amplitude
L – Coil inductance	Estimate	Shifts coil mode frequency

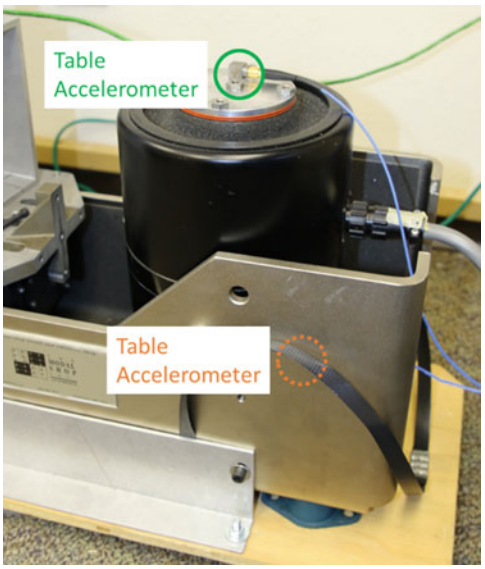

Fig. 15.4 Small shaker model validation test setup

15.4 Shaker Model Validation and Updating

The model developed must be validated using data from the shaker itself. This is especially important, as only 5 of the 12 parameters are known. To capture the behavior of the shaker, a test was set up to measure the three FRFs of interest. The shaker characterized was a Modal Shop (TMS) K2075E dual-purpose 75lbf shaker. Two triaxial accelerometers were placed on the shaker, with one on the armature table and one on the body of the shaker, as shown in Fig. 15.4. The accelerometer on the body is located on the black body of the shaker but obscured by the slip table housing. The amplifier's built-in current monitor was used to measure the current supplied, and a voltage probe was attached to the amplifier output terminal to measure the voltage input supplied. In addition to the voltage from the amplifier, the drive voltage from the data acquisition unit (DAQ) was measured. This setup captures nearly all the degrees of freedom in the model, but the armature coil is inaccessible for direct measurement.

The test profile used was a flat 1 g RMS power spectral density (PSD) from 1 Hz to 6500 Hz with a 1 Hz frequency spacing to characterize the full range of the shaker's dynamics. The frequency limits were based on the limitations of the equipment used, the expected dynamics of the system, and the controllability of the profile. The test was controlled using the Siemens LMS Testlab 2021.1 software's Random Vibration control module. The test was run both open loop and closed loop to observe any effects of the controller on the FRFs. For the closed loop control, the test was controlled on the Z-axis of the table accelerometer. The data was collected in the time-domain using a sample rate of 25.6 kHz.

The results from the characterization test closely matched the shape of the expected curves from the literature. The three FRFs were calculated from the time data collected using a two second Hanning window with a 50% overlap. Figure 15.5 shows the results of the test with the model results. The shaker impedance, which is the measured voltage over the measured current across the frequency range, is shown in the real-imaginary form, while the other two FRFs are displayed in magnitude-phase form. Very little difference was seen between the open and closed loop controls, with less than 5% difference in magnitude for all three FRFs. The closed loop results are displayed in the figure. Two modes, the suspension and coil modes, are clearly visible on the plots, but the isolation mode is not. It is possible that either the mode is out of the range of interest or does not have sufficient amplitude to be viewed. In either case, this indicates that the model may be successful without including the body degree of freedom.

The data collected in the characterization test was then used for updating the model. First, the model was updated by hand to get an approximate fit of the data and provide a starting point for an optimization that would determine the final fit of the model. Using the results of the parameter sensitivity study, model parameters were chosen by trial and error and evaluated compared to the data. Table 15.2 shows the values chosen for the hand-fit of the model. An imaginary component was added to the inductance, as Mayes et al. [3] found their amplifier exhibited a fixed phase difference between the current and voltage. This phase difference results in a real component of the impedance increases proportional with frequency. Making the inductance complex compensates for this, it is not indicative of the physical phenomenon occurring.

The hand-fit model was then used as the initial state for the optimization to make the final model fit. MATLAB's *fmincon* algorithm was used for the optimization. *fmincon* is a gradient-based nonlinear constrained optimization algorithm. The

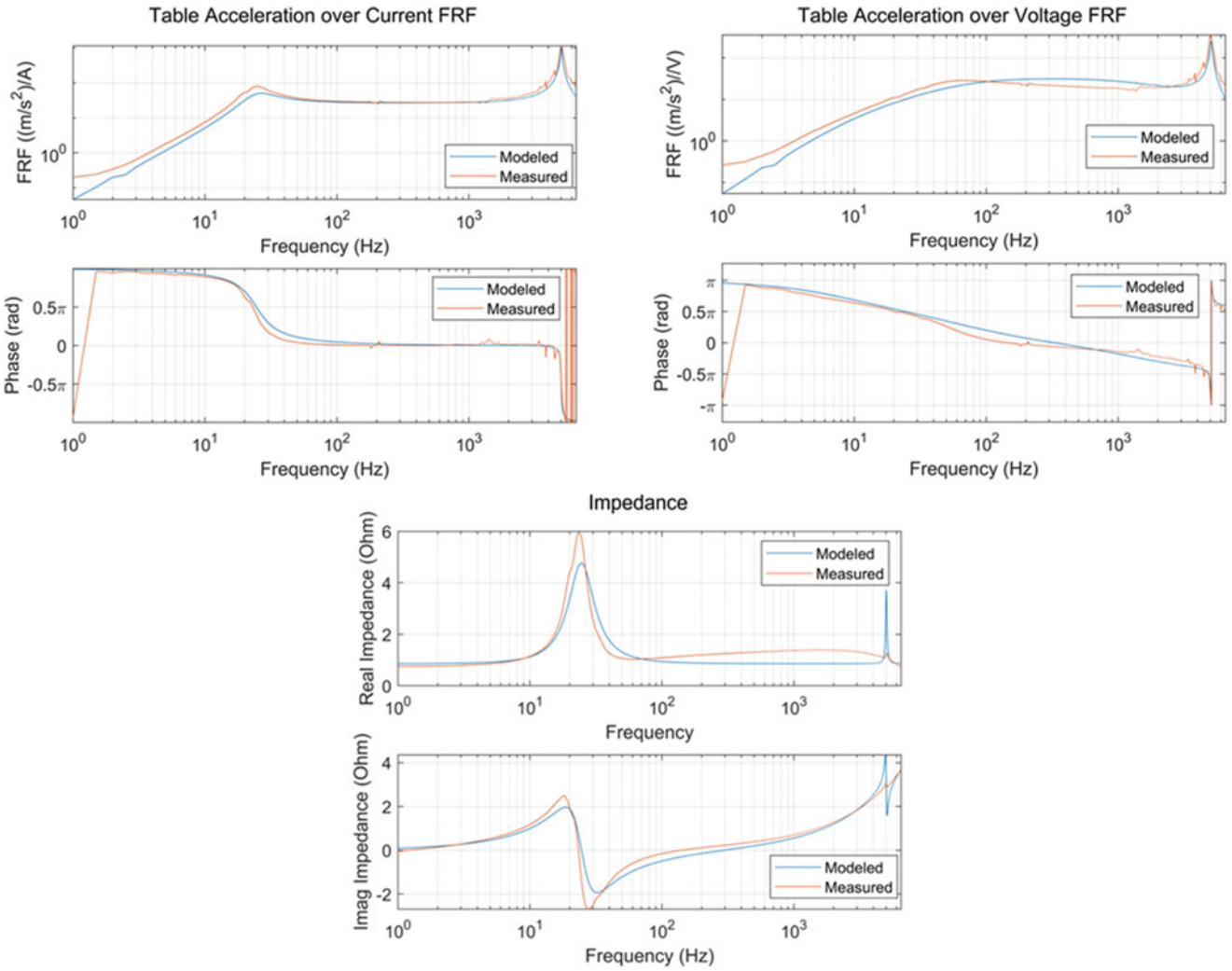

Fig. 15.5 Comparison of the updated model FRFs to the measured FRFs of the shaker

Table 15.2 Chosen model parameters

Parameter	Hand fit value	Updated value	Units
Body mass	15.55	15.55 (fixed)	kg
Table mass	0.40	0.40 (fixed)	kg
Coil mass	0.05	0.05 (fixed)	kg
Body damping	100	0.00451	N/(m/s)
Flexure damping	20	37.8	N/(m/s)
Coil damping	40	39.7	N/(m/s)
Body stiffness	10,000	3.34e3	N/m
Flexure stiffness	10,500	10,500 (fixed)	N/m
Coil stiffness	4.50e7	4.72e7	N/m
Resistance	0.86	0.86 (fixed)	Ω
Real (inductance)	0.00012	9.46E-05	H
Imag (inductance)	2.00E-05	5.22E-14	H
Coupling coefficient	12	13.2	–

objective function used was a weighted sum of the root mean square errors of the real and imaginary parts of each FRF across all frequency lines.

$$e_{\text{FRF}} = \sqrt{\frac{\sum_{n=1}^{N} \sum \left(\text{real}\left(h_{n,\text{model}}\right) - real\left(h_{n,\text{measured}}\right)\right)^2}{N}} + \sqrt{\frac{\sum_{n=1}^{N} \sum \left(\text{imag}\left(h_{n,\text{model}}\right) - real\left(h_{n,\text{measured}}\right)\right)^2}{N}} \tag{15.12}$$

$$e_{\text{model}} = a_1 e_{\text{Impedance}} + a_2 e_{\text{Accel-Voltage}} + a_3 e_{\text{Accel-Current}} \tag{15.13}$$

In these equations, h_n is the value of the FRF at the nth frequency line, N is the total number of frequency lines, and a_i is the weight assigned to the RMS error of that FRF. Weights were assigned to compensate for the varying magnitudes of the FRFs investigated, otherwise the acceleration-current FRF dominates the error. The five model parameters that could be determined from the specification sheet of the shaker and measurements (body mass, table mass, coil mass, flexure stiffness, and resistance) were held fixed while the remaining seven parameters were allowed to vary. The only constraint used was that parameters must be nonnegative. Table 15.2 also shows the parameter values determined from the optimization, and Fig. 15.5 compares the calculated FRFs from these parameters to the measured data. Most of the model parameters were not drastically changed; however, the damping and stiffness related to the body degree of freedom did. This is likely because the isolation mode is not clearly seen in the measured data and had little impact on the value of the objective function. The imaginary portion of the inductance approached zero, indicating the phase difference was likely not seen in the equipment used.

15.5 BARC Base Modal Testing

A generic DUT was needed for assessing the effectiveness of using experimental dynamic substructuring for shaker capability estimation. The base of the Box Assembly and Removable Component (BARC) was chosen as the DUT. The BARC is a common challenge testbed used within the dynamic environments testing community. The base of the BARC, i.e., without the removable component, was used because it does not contain any bolted joints, which are dynamically complex and difficult to characterize.

A multi-reference impact test (MRIT) was performed to develop a modal model of the BARC base. The test was performed with the BARC suspended from a modal test stand using fishing wire to approximate a free-free boundary condition. A combination of uniaxial and triaxial accelerometers were used, totaling 12 sensors and 24 reference channels. The extensive instrumentation was chosen for possible future applications of a virtual point transformation to aid the results of the FBS, where the motion in 6-DOFs at virtual connection points is estimated by making measurements around each point [14]. A PCB 086C02 modal impact hammer was used for excitation. All data were collected using a Siemens LMS SCADAS Mobile DAQ and Siemens Simcenter Testlab software. A bandwidth of 8192 Hz with 16,384 spectral lines was used, resulting in a two second acquisition window. The structure is very lightly damped and continued to resonate after the acquisition window ended, causing low-frequency leakage, so a 30% exponential decay window was applied to the data collected. A 5% force-exponential window was used on the input. Five averages were collected for each FRF. Figure 15.6 shows the test setup.

A driving point measurement is needed at each of the connection points for substructure coupling. In addition, each point of interest anywhere else on the structure also requires a driving point. These points could be potential control points that must be evaluated for estimating shaker capability. The results of the driving point measurements are a 24 × 24 × 16384 FRF matrix that was used for modal parameter estimation.

Modal parameter estimation was performed using the orthogonal polyreference, or OPoly, tool in the third-party MATLAB toolbox, IMAT 7.9.0, developed by ATA Engineering. First, the full range of interest, from 1 Hz up to 6500 Hz, was attempted for modal parameter estimation. However, the parameter estimation algorithm struggled with fitting such a large frequency range. This difficulty is likely because the test conducted did not well characterize the rigid body modes which occurred between 0 Hz and 10 Hz. Additionally, the input spectrum achieved by the hammer begins to roll off significantly after 6000 Hz. Instead, a shorter range was fit, from 50 Hz to 1960 Hz, which spanned from the first elastic mode up to the eleventh.

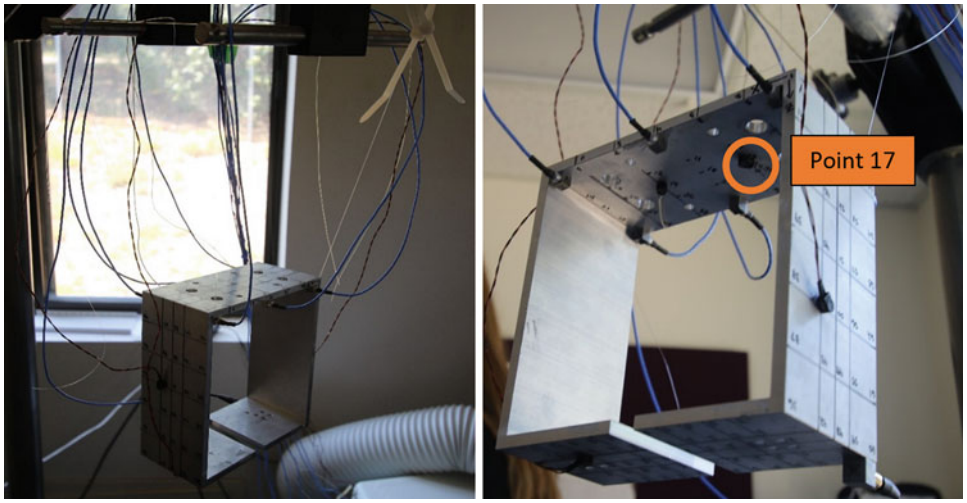

Fig. 15.6 Modal impact test setup

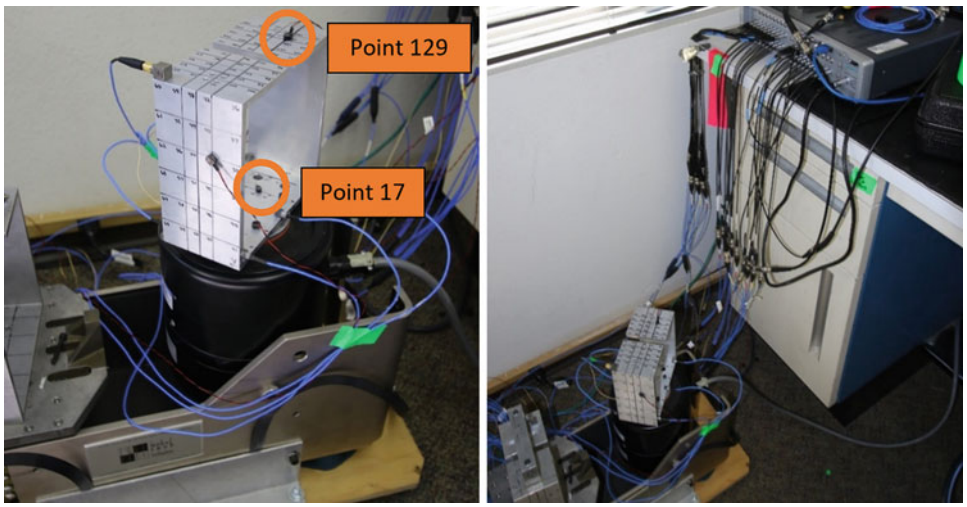

Fig. 15.7 Setup of the substructure coupling validation test

15.6 Substructuring Analysis and Results

The experimental model of the BARC base was analytically coupled to the analytical model of the small shaker using Eq. 15.8. The synthesized FRFs of the BARC base are the data used for the substructure coupling analysis, because they are analytically derived from the estimated modal parameters and are less noisy. The inversion in the LM-FBS coupling equation causes the formula to be susceptible to noise in the FRFs used. Similarly, the FRFs calculated from the model of the shaker are used. Points 17 and 19, located on the base between the mounting holes, were chosen as the analytical coupling points on the BARC base and were coupled with the table DOF of the shaker model. This creates two interface conditions. Using Eq. 15.8, the coupled FRF matrix is then calculated on a frequency line basis. The frequency range of the modal parameter estimation, 50 Hz to 1960 Hz, with a 1 Hz spacing was used.

The substructuring analysis must be experimentally validated, so a random vibration test of the BARC base attached to the shaker was conducted. This test utilized the same instrumentation setup on the BARC base as in the modal test, but also measured the current and voltage supplied by the amplifier to the shaker. The test was again run using the Random Vibration control module of Siemens Simcenter Testlab. The test was conducted from 10 Hz to 6000 Hz with a 2 Hz frequency resolution. A sample rate of 25.6 kHz was used. Figure 15.7 shows a setup of the test. Similar to the test analysis performed for the shaker model validation, the impedance, acceleration over voltage, and acceleration over current FRFs were calculated from the time history data collected and can be found in Fig. 15.8.

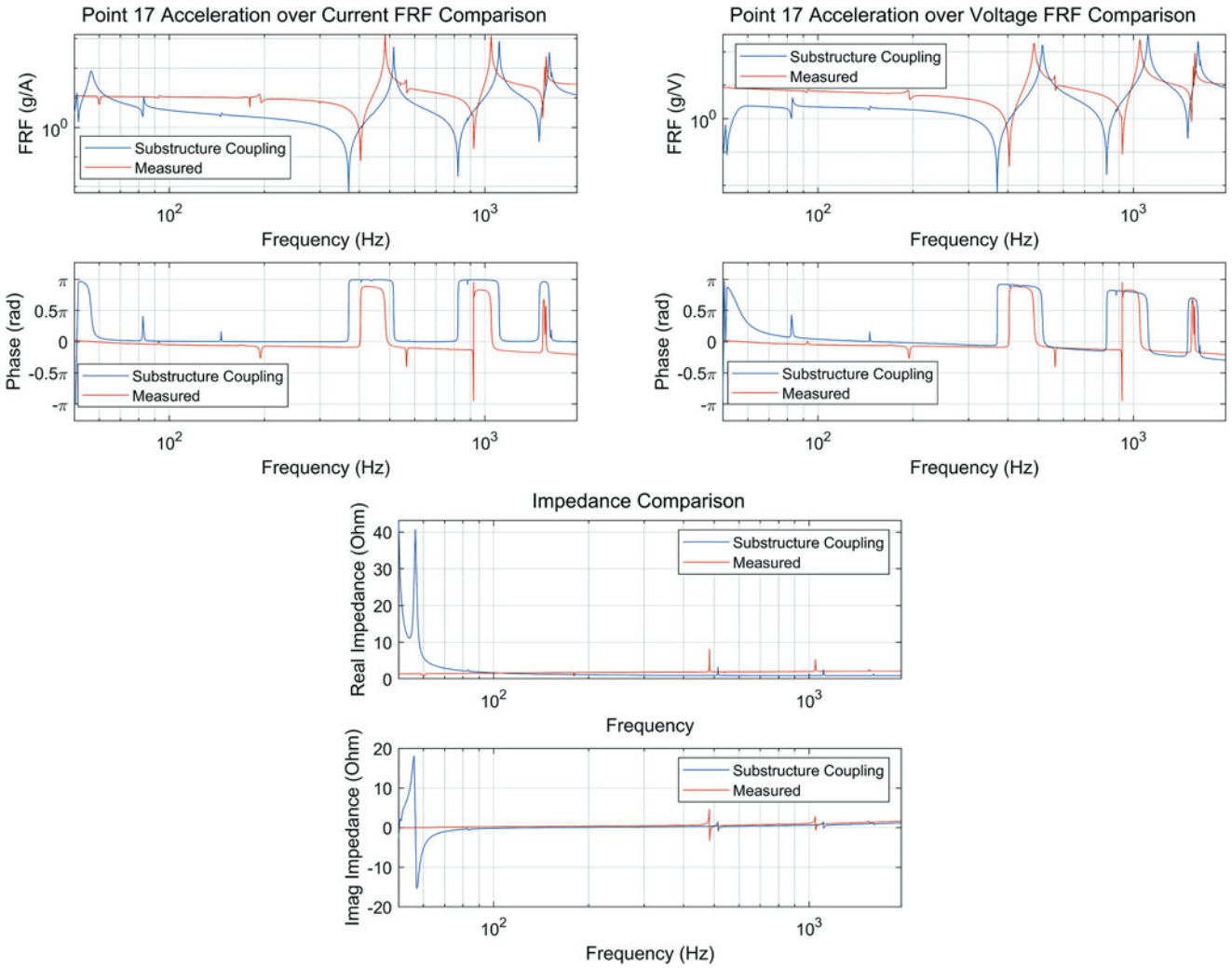

Fig. 15.8 FRFs at Point 17 estimated from substructure coupling compared to measured FRFs at Point 17

The results of the coupling shown in Figs. 15.8 and 15.9 are compared to the validation test results. The results of the substructuring analysis are not perfect but indicate that the method could be used for predicting shaker capability, with some improvement. The modeled impedance matches the amplitude of the measured impedance but sees large erroneous peaks at the low frequency. Points 17 and 129, both uniaxial accelerometers measuring in the vertical direction, were used for comparisons. Point 17 was a coupling point between the modal model of the BARC base and shaker model, while point 129 is located on top of the BARC base. In both cases, the model has the same overall shape as the measured FRFs for both points, though the resonant frequencies are generally underestimated in the lower frequency range (50 Hz to 300 Hz) and overestimated in the upper frequency range (300 Hz to 1960 Hz). These upper frequency range resonances are also overestimated in the impedance. The overall magnitude of the acceleration FRFs also appears to be too low.

15.7 Conclusions

The results of this work show promise that shaker capability could be estimated for individual test setups following this same process of modeling the shaker, experimentally characterizing the DUT, and potentially even fixturing, and then, coupling all the components together with dynamic substructuring. Once the FRFs of the system are calculated, they can be inverted and used as filters to determine the electrical input spectra required to achieve an acceleration PSD test specification. The

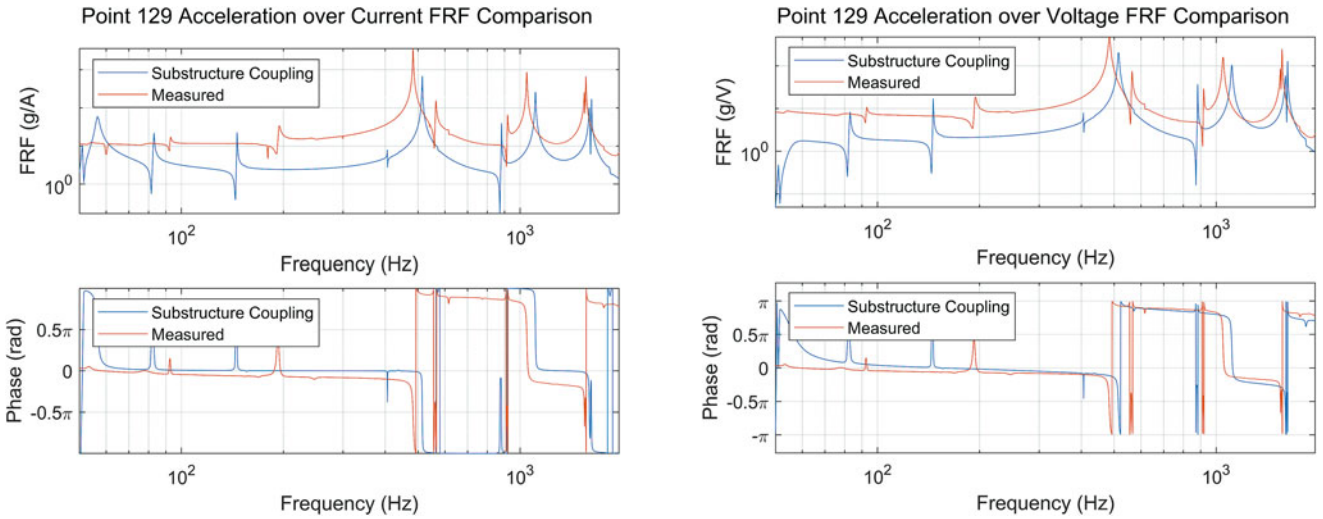

Fig. 15.9 FRFs at Point 129 estimated from substructure coupling compared to measured FRFs at Point 129

shaker model adequately captured the shaker's dynamics, and the modal parameter estimation was successful in the limited range that was fit. Based on the FRFs calculated from the measured data on the shaker, it may be possible to remove the body degree of freedom, as the isolation mode was not clearly visible. This may also improve the efficiency of the optimization used to update the model by reducing the solution space.

The results of the substructuring analysis could see significant improvement. A very simple method of experimental dynamic substructuring was used, and the coupling points chosen, while in the middle of the shaker-BARC interface, were not at all co-located with the physical connection points. More advanced techniques for substructuring, such as using a virtual point transformation to couple at the physical connection points and with more degrees of freedom, could improve results. In addition, the narrow dynamic range fit for the modal model did not include the shaker's armature resonance, which often introduces the most difficulties to testing. Capturing a wider range would better describe the capabilities of the shaker at all operating ranges, and significantly improve the usefulness of this method. A better fit of the lower range may also improve the results of the substructuring, as the rigid body motion of the BARC base was not captured.

Acknowledgments This work was funded by the Delivery Environments program at Los Alamos National Laboratory, under the Office of Engineering and Technology Maturation.

References

1. Lang, G.F., Snyder, D.: Understanding the physics of electrodynamic shaker performance. Sound Vib. **35**(10), 24–33 (2001)
2. Schultz, R.: Calibration of Shaker Electro-mechanical Models. In: Proceedings of the 38th IMAC (2020)
3. Mayes, R. L., Ankers, L., Daborn, P. M., Moulder, T., Ind, P.: Optimization of shaker locations for multiple shaker environmental testing. In: Proceedings of IMAC XXXVII, the 37th International Modal Analysis Conference (2019)
4. Ricci, S., Peeters, B., Fetter, R., Boland, D., Debille, J.: Virtual Shaker Testing for Predicting and Improving Vibration Test Performance. In: Proceedings of the IMAC-XXVII (2009)
5. Manzato, S., Bucciarelli, F., Arras, M., Coppotelli, G., Peeters, B., Carrella, A.: Validation of a Virtual Shaker Testing approach for improving environmental testing performance. In: Proceedings of ISMA 2014 - International Conference on Noise and Vibration Engineering (2014)
6. Smallwood, D. O.: Characterizing Electrodynamic Shakers. In: Annual Technical Meeting and Exposition of the Institute of Environmental Sciences (1997)
7. Tiwari, N., Puri, A., Saraswat, A.: Lumped parameter modelling and methodology for extraction of model parameters for an electrodynamic shaker. J. Low Freq. Noise Vib. Active Control. **36**(2), 99–115 (2017)
8. McConnell, K.: Vibration exciters. In: Vibration Testing: Theory and Practice, pp. 363–440. John Wiley & Sons (1995)
9. Varoto, P.S., De Oliveira, L.P.R.: Interaction between a vibration exciter and the structure under test. Sound Vib. (October 2002)
10. Hoffait, S., Marin, F., Simon, D., Peeters, B., Golinval, J.C.: Measured-based shaker model to virtually simulate vibration sine test. Case Stud. Mech. Syst. Signal Process. **4**, 1–7 (2016)
11. de Klerk, D., Rixen, D.J., Voormeeren, S.N.: General framework for dynamic substructuring: history, review, and classification of techniques. AIAA J. **6**(5), 1169–1181 (2008)

12. de Klerk, D., Rixen, D.J., de Jong, J.: The Frequency Based Substructuring (FBS) Method reformulated according to the Dual Domain Composition Method. In: Proceedings of the XXIV International Modal Analysis Conference, January (2006)
13. Jetmundsen, B.: On Frequency Domain Methodologies for Structural Modification and Subsystem Synthesis, Ph.D. thesis. Rensselaer Polytechnic Institute, Troy (1986)
14. van der Seijs, M. V., van den Bosch, D. D., Rixen, D. J., de Klerk, D.: An improved methodology for the virtual point transformation of measured frequency response functions in dynamic substructuring. In: 4th ECCOMAS Thematic Conference on Computational Methods in Structural Dynamics and Earthquake Engineering, pp. 4334–4347 (2013)